# 論文 / 著書情報
# Article / Book Information

| | |
|---|---|
| 題目(和文) | 格子QCDによるチャームバ　リオンの電磁形状因子の研究 |
| Title(English) | ELECTROMAGNETIC FORM FACTORS OF CHARMED BARYONS IN LATTICE QCD |
| 著者(和文) | CanKadir Utku |
| Author(English) | Utku Can |
| 出典(和文) | 学位:博士(理学),<br>学位授与機関:東京工業大学,<br>報告番号:甲第10400号,<br>授与年月日:2017年3月26日,<br>学位の種別:課程博士,<br>審査員:岡 眞,伊藤 克司,山口 昌英,柴田 利明,西田 祐介,Guray Erkol |
| Citation(English) | Degree:Doctor (Science),<br>Conferring organization: Tokyo Institute of Technology,<br>Report number:甲第10400号,<br>Conferred date:2017/3/26,<br>Degree Type:Course doctor,<br>Examiner:,,,,, |
| 学位種別(和文) | 博士論文 |
| Category(English) | Doctoral Thesis |
| 種別(和文) | 要約 |
| Type(English) | Outline |

# ELECTROMAGNETIC FORM FACTORS OF CHARMED BARYONS IN LATTICE QCD

## (格子QCDによるチャームバリオンの電磁形状因子の研究)

BY
K. UTKU CAN

THESIS OUTLINE

SUPERVISOR
PROF. DR. MAKOTO OKA

FEBRUARY 2017

**Abstract**

The electromagnetic form factors of spin-1/2 $\Sigma_c$, $\Xi_{cc}$, $\Omega_c$, $\Omega_{cc}$ and spin-3/2 $\Omega$, $\Omega_c^*$, $\Omega_{cc}^*$, $\Omega_{ccc}$ baryons are computed in full QCD on $32^3$ x 64 PACS-CS lattices. For spin-1/2 baryons, their electric and magnetic charge radii as well as their magnetic moments are extracted. Extrapolated physical point results show that the charge radii and magnetic moments are smaller compared to those of, e.g., proton. Investigating the individual quark contributions suggests that the existence of the heavy charm quark is responsible of such decrease. For spin-3/2 baryons, their electric charge radii and magnetic moments from the E0 and M1 multipole form factors are extracted. Results for the electric quadrupole form factor, E2, are also provided. Quark sector contributions are computed individually for each observable and then combined to obtain the baryon properties. Charm quark contributions are observed to be systematically smaller compared to the strange quark contributions in case of the charge radii and magnetic moments. E2 moments of the $\Omega_{cc}^*$ and $\Omega_{ccc}$ are estimated significantly enough to show that their electric charge distributions are deformed. A comparison between the properties of the spin-1/2 counterparts of the $\Omega_c^*$ and $\Omega_{cc}^*$ baryons is presented.

If you want to refer to this document please use the listed citations instead:

- Chapter 1: K. U. Can, G. Erkol, B. Isildak, M. Oka, Toru T. Takahashi, *Electromagnetic structure of charmed baryons in Lattice QCD*, **PoS LATTICE2014 (2015) 157**.
- Chapter 2: K. U. Can, G. Erkol, M. Oka, Toru T. Takahashi, *Electromagnetic structure of charmed baryons - extended to spin-3/2*, **PoS LATTICE2015 (2016) 133**.

# Chapter 1

# Spin-1/2 Baryons

## 1.1 Introduction

The electric and magnetic properties of the hadrons can be probed by the electromagnetic form factors and valuable information can be extracted, such as their sizes or distributions of their components. The framework of lattice QCD enables us to determine such form factors starting from quark and gluon degrees of freedom. In our previous works we have found that the existence of a charm quark drives the charge radii and magnetic moments of the hadrons to smaller values [1, 2]. Yet it is interesting to see how the charge radii are affected as the light quark gets heavier as in the case of replacing the $u/d$ quark by an $s$ quark.

In this work, we report our results for the singly charmed $\Sigma_c^{(0,++)}(cdd, cuu)$, $\Omega_c^0(css)$ baryons and the doubly charmed $\Xi_{cc}^{(+,++)}(ccd, ccu), \Omega_{cc}^{+}(ccs)$ baryons. In particular we compute the electromagnetic form factors and extract the electric and magnetic charge radii, and the magnetic moments of these baryons.

## 1.2 Lattice Formulation and Setup

Electromagnetic form factors can be calculated by considering the baryon matrix elements of the electromagnetic vector current $V_\mu = \sum_q e_q \bar{q}(x)\gamma_\mu q(x)$, where $q$ runs over the quark content of the given baryon. The matrix element can be written in the following form

$$\langle B(p)|V_\mu|B(p')\rangle = \bar{u}(p)\left[\gamma_\mu F_{1,B}(q^2) + i\frac{\sigma_{\mu\nu}q^\nu}{2m_B}F_{2,B}(q^2)\right]u(p), \tag{1.1}$$

where $q_\mu = p'_\mu - p_\mu$ is the transferred four-momentum. Here $u(p)$ denotes the Dirac spinor for the baryon with four-momentum $p^\mu$ and mass $m_B$. The Sachs form factors $F_{1,B}(q^2)$ and $F_{2,B}(q^2)$ are related to the electric and magnetic form factors by

$$G_{E,B}(q^2) = F_{1,\mathcal{B}}(q^2) + \frac{q^2}{4m_B^2} F_{2,\mathcal{B}}(q^2), \qquad G_{M,B}(q^2) = F_{1,\mathcal{B}}(q^2) + F_{2,\mathcal{B}}(q^2). \tag{1.2}$$

Our method of computing the matrix element in Eq. (1.1), which was employed to extract the nucleon electromagnetic form factor, follows closely that of Ref.[3]. Using the following ratio

$$\begin{aligned} R(t_2, t_1; \mathbf{p}', \mathbf{p}; \Gamma; \mu) = & \frac{\langle F^{BV_\mu B'}(t_2, t_1; \mathbf{p}', \mathbf{p}; \Gamma)\rangle}{\langle F^{BB}(t_2; \mathbf{p}'; \Gamma_4)\rangle} \\ & \times \left[ \frac{\langle F^{BB}(t_2 - t_1; \mathbf{p}; \Gamma_4)\rangle \langle F^{BB}(t_1; \mathbf{p}'; \Gamma_4)\rangle \langle F^{BB}(t_2; \mathbf{p}'; \Gamma_4)\rangle}{\langle F^{BB}(t_2 - t_1; \mathbf{p}'; \Gamma_4)\rangle \langle F^{BB}(t_1; \mathbf{p}; \Gamma_4)\rangle \langle F^{BB}(t_2; \mathbf{p}; \Gamma_4)\rangle} \right]^{1/2}, \end{aligned} \tag{1.3}$$

where the baryonic two-point and three-point correlation functions are respectively defined as:

$$\langle F^{BB}(t; \mathbf{p}; \Gamma_4)\rangle = \sum_{\mathbf{x}} e^{-i\mathbf{p}\cdot\mathbf{x}} \Gamma_4^{\alpha\alpha'} \times \langle \mathrm{vac}|T[\eta_B^\alpha(x)\bar{\eta}_B^{\alpha'}(0)]|\mathrm{vac}\rangle, \tag{1.4}$$

$$\langle F^{BV_\mu B'}(t_2, t_1; \mathbf{p}', \mathbf{p}; \Gamma)\rangle = -i \sum_{\mathbf{x_2}, \mathbf{x_1}} e^{-i\mathbf{p}\cdot\mathbf{x_2}} e^{i\mathbf{q}\cdot\mathbf{x_1}} \Gamma^{\alpha\alpha'} \langle \mathrm{vac}|T[\eta_B^\alpha(x_2) V_\mu(x_1) \bar{\eta}_{B'}^{\alpha'}(0)]|\mathrm{vac}\rangle, \tag{1.5}$$

with $\Gamma_i = \gamma_i\gamma_5\Gamma_4$ and $\Gamma_4 \equiv (1+\gamma_4)/2$. The baryon interpolating fields are chosen, similarly to that of the octet baryons, as

$$\begin{aligned} \eta_{\Sigma_c}(x) &= \epsilon^{ijk}[\ell^{Ti}(x) C\gamma_5 c^j(x)]\ell^k(x), \quad \eta_{\Omega_c}(x) = \epsilon^{ijk}[s^{Ti}(x) C\gamma_5 c^j(x)]s^k(x), \\ \eta_{\Xi_{cc}}(x) &= \epsilon^{ijk}[c^{Ti}(x) C\gamma_5 \ell^j(x)]c^k(x), \quad \eta_{\Omega_{cc}}(x) = \epsilon^{ijk}[c^{Ti}(x) C\gamma_5 s^j(x)]c^k(x), \end{aligned} \tag{1.6}$$

where $\ell = u$ for the doubly charged $\Xi_{cc}^{++}(ccu)/\Sigma_c^{++}(cuu)$ and $\ell = d$ for the singly charged $\Xi_{cc}^{+}(ccd)/\Sigma_c^{+}(cdd)$ baryons. Here $i$, $j$, $k$ denote the color indices and $C = \gamma_4\gamma_2$. $t_1$ is the time when the external electromagnetic field interacts with a quark and $t_2$ is the time when the final baryon state is annihilated. When $t_2 - t_1$ and $t_1 \gg a$, the ratio in Eq. (1.3) reduces to the desired form

$$R(t_2, t_1; \mathbf{p}', \mathbf{p}; \Gamma; \mu) \xrightarrow[t_2 - t_1 \gg a]{t_1 \gg a} \Pi(\mathbf{p}', \mathbf{p}; \Gamma; \mu). \tag{1.7}$$

We extract the form factors $G_{E,B}(q^2)$ and $G_{M,B}(q^2)$ by choosing appropriate combinations

of Lorentz direction $\mu$ and projection matrices $\Gamma$:

$$\Pi(\mathbf{0}, -\mathbf{q}; \Gamma_4; \mu = 4) = \left[\frac{(E_B + m_B)}{2E_B}\right]^{1/2} G_{E,B}(q^2), \tag{1.8}$$

$$\Pi(\mathbf{0}, -\mathbf{q}; \Gamma_j; \mu = i) = \left[\frac{1}{2E_B(E_B + m_B)}\right]^{1/2} \epsilon_{ijk}\, q_k\, G_{M,B}(q^2). \tag{1.9}$$

Here, $G_{E,B}(0)$ gives the electric charge of the baryon. Similarly, the magnetic moment can be obtained from the magnetic form factor $G_{M,B}$ at zero momentum transfer.

We run our simulations on $32^3 \times 64$, 2+1-flavor configurations generated by the PACS-CS Collaboration [4] using the Clover fermion action and the Iwasaki gauge action. We use the gauge configurations at $\beta = 1.90$ with the Clover coefficient $c_{SW} = 1.715$, which give a lattice spacing of $a = 0.0907(13)$ fm ($a^{-1} = 2.176(31)$ GeV). The simulations are carried out with four different hopping parameters for the light sea and valence quarks, $\kappa^{sea}_{u,d}$, $\kappa^{val}_{u,d}$=0.13700, 0.13727, 0.13754 and 0.13770, which correspond to pion masses of approximately 702, 570, 411, and 296 MeV. The strange quark mass is fixed to its physical value at $\kappa^{s}_{sea} = 0.13640$. In order to be consistent with the sea quarks we use the clover action for the u, d and s valence quark propagators and we take $\kappa^{q}_{sea} = \kappa^{q}_{val}$.

We employ a wall method [1], which provides a simultaneous study of all the hadrons we are considering. The source is Gaussian smeared in a gauge-invariant manner. The source-sink separation is chosen to be 12 lattice units in the temporal direction. In the case of $u$, $d$ and $s$ quarks, we choose the smearing parameters so as to give a root-mean-square radius of $\langle r_l \rangle \sim 0.5$ fm. As for the charm quark, we adjust the smearing parameters to obtain $\langle r_c \rangle = \langle r_l \rangle / 3$.

For the charm quarks, we apply the Fermilab method [5] in the form employed by the Fermilab Lattice and MILC Collaborations [6, 7]. In this simplest form of the Fermilab method, the clover coefficients $c_E$ and $c_B$ in the action are set to the tadpole-improved value $1/u_0^3$, where $u_0$ is the average link. Following the approach in Ref. [8], we estimate $u_0$ to be the fourth root of the average plaquette. We tuned the charm-quark hopping parameter to $\kappa_c = 0.1246$ by comparing the experimental spin-averaged static masses of charmonium and heavy-light mesons with our lattice results [9].

For each $\kappa^{ud}_{sea}$ value, we perform our measurements on 100, 100, 150 and 170 different configurations for the $\Sigma_c$ and $\Xi_{cc}$ and 100, 100, 100 and 130 different configurations for the $\Omega_c$ and $\Omega_{cc}$ baryons. In order to increase the statistics we use multiple source-sink pairs for the $\Sigma_c$ and $\Xi_{cc}$ baryons. We insert momentum through the current up to nine units: $(|p_x|, |p_y|, |p_z|)$=(0,0,0), (1,0,0), (1,1,0), (1,1,1), (2,0,0), (2,1,0), (2,1,1), (2,2,0), (2,2,1) and average over equivalent momenta in the case of electric form factor. For the magnetic form factor we average over all equivalent combinations of spin projection, Lorentz component

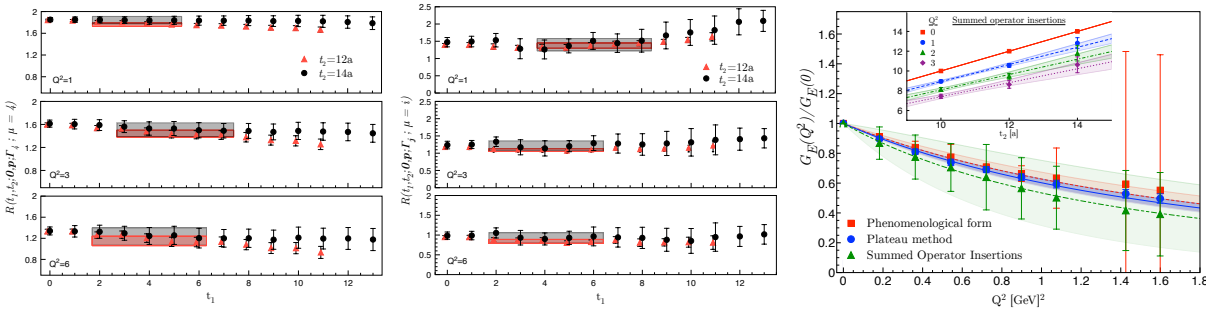


(a) (b)

Figure 1.1: **(a)** The ratio in Eq. 1.3 as function of the current insertion time, $t_1$, for the electric (left) and magnetic (right) form factor of $\Xi_{cc}$ with $t_2 = 12a$ and $t_2 = 14a$. We show statistics over 30 configurations for three illustrative momentum-transfer values. The data for $t_2 = 12a$ are slightly shifted to left for clear viewing. **(b)** A comparison of the electric form factor of $\Xi_{cc}$ for the heaviest quark mass, as obtained using a simple plateau fit, the phenomenological fit form and the summation method. The small panel depicts the summed operator insertions for three time separations and for the first four momentum insertions with their linear fits.

and momentum indices. We use the point-split lattice current, $V_\mu = 1/2[\overline{q}(x+\mu)U^\dagger_\mu(1+\gamma_\mu)q(x) - \overline{q}(x)U_\mu(1-\gamma_\mu)q(x+\mu)]$, which is conserved by the Wilson fermions, therefore does not require any renormalisation. All statistical errors are estimated by the single-elimination jackknife analysis and the $\chi^2$ p-values are used to test the goodness of fits.

In our simulations, the source-sink time separation is fixed to 1.09 fm ($t_2 = 12a$). There are works in the literature for the nucleon axial and electromagnetic form factors [3, 10] as well as for the $\Omega^-$ electromagnetic form factors [11] which finds a separation of 1 fm between the source and sink is sufficient to avoid excited-state contaminations. To check that a separation of $t_2 = 12a$ is sufficient for the charmed baryons, we compare our electric and magnetic results for the form factors of $\Xi_{cc}$ with $t_2 = 12a$ and $t_2 = 14a$ as shown in Fig. 1.1a. The plateau values obtained from the two time separations are consistent with each other, implying that the shorter source-sink time separation is sufficient. Other baryons we study exhibit a similar behaviour, therefore we use the shorter separation *i.e.* $t_2 = 12a$ in all of our analysis.

To further ensure that the ground state baryon is isolated from the excited-state contaminations we performed a secondary analysis and fitted the ratio in Eq. (1.3) to a phenomenological form

$$R(t_2, t_1) = G_{E,M} + b_1\, e^{-\Delta t_1} + b_2\, e^{-\Delta(t_2 - t_1)}, \tag{1.10}$$

where $\Delta$ is the energy gap between the ground and the excited state. Since the energy gap is not known for charmed baryons we leave $\Delta$ as a free parameter together with $b_1$

and $b_2$, which yields a larger uncertainty for $G_{E,M}$.

In Fig. 1.1b we compare the electric form factor of $\Xi_{cc}$ as obtained using a simple plateau fit and the phenomenological fit form in Eq. (1.10), for the heaviest quark mass. The two fit forms give completely consistent results, with the phenomenological fit form having twice as large errors. We have not been able to obtain a good fit to the phenomenological form for the magnetic form factors. The statistical errors in the parameters of the fit to $R(t_2, t_1)$ are too large to allow a precise determination of $G_M$. Therefore, we use solely a plateau fit in extracting the ground state matrix elements of electric and magnetic form factors. We show all the plateau fits in Ref. [9].

We also consider the *summed operator insertions* method [12] with three source-sink separations, namely for $t_2 = 10a$, $t_2 = 12a$ and $t_2 = 14a$ (for the heaviest quark mass and using 30 configurations). Since this is a computationally extensive method we have employed it as an exploratory case in this work. Fig. 1.1b depicts a comparison of the summation method with the other methods also. In general, the data are consistent within the errors but the statistical errors for the summation method is still large. We intend to study the summation method further with increased statistics in a future work.

## 1.3 Results and Discussion

We use the dipole form to describe the $Q^2$ dependence of the baryon form factors:

$$G_{E,M}(Q^2) = G_{E,M}(0)/(1 + Q^2/\Lambda^2_{E,M})^2. \tag{1.11}$$

In Fig. 1.2 we only give the electric form factors of $\Sigma_c^{++}$, $\Xi_{cc}^{++}$ and $\Omega_{cc}^{+}$, as normalized with their electric charges, to illustrate our fits. Fits on all different $\kappa_{u,d}$ lattices are shown in the figure. The magnetic form factors of $\Xi_{cc}^{+}$, $\Omega_{cc}^{+}$, $\Omega_c^0$, $\Sigma_c^0$ and $\Sigma_c^{++}$ baryons can be found in Ref. [9].

We can extract the electric/magnetic charge radii of the baryons from the slope of the form factor at $Q^2 = 0$ by, $\langle r^2 \rangle = -\frac{6}{G(0)} \frac{d}{dQ^2} G(Q^2)\big|_{Q^2=0}$. Using the dipole form in Eq. (1.11), we get $\langle r^2_{E,M} \rangle = 12/\Lambda^2_{E,M}$. Then the charge radii can be directly calculated using the values of dipole masses as obtained from our simulations.

The magnetic moment is defined as $\mu_B = G_M(0)e/(2m_B)$ in natural units. We obtain $G_M(0)$ by extrapolating the lattice data to $Q^2 = 0$ via the dipole form in Eq. (1.11) as explained above. We evaluate the magnetic moments in nuclear magnetons using the relation $\mu_B = G_M(0)\,(e/2m_B) = G_M(0)\,(m_N/m_B)\,\mu_N$, where $m_N$ is the physical nucleon mass and $m_B$ is the baryon mass as obtained on the lattice.

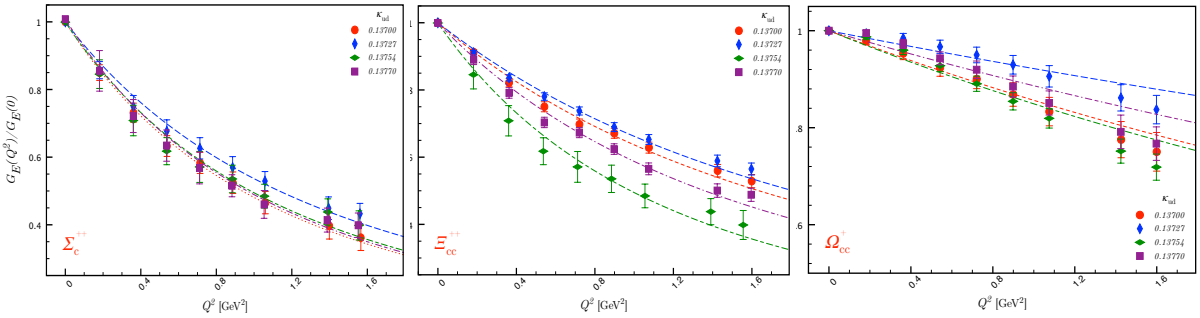

Figure 1.2: The electric form factors of $\Sigma_c^{++}$,$\Xi_{cc}^{++}$ and $\Omega_{cc}^{+}$ as normalized with their electric charges as functions of $Q^2$, for all the quark masses we consider. The dots mark the lattice data and the curves show the best fit to the dipole form in Eq. (1.11).

In Table 1.1, we give the electric and magnetic charge radii in fm$^2$, and the magnetic moments ($\mu_B$) in nuclear magnetons at the chiral point. These numerical values with their chiral extrapolations and results at each light quark kappa can be found in Ref. [9]. Some select chiral extrapolations are given in Fig. 1.3 for illustration. We used three fit forms that are constant, linear and quadratic in $m_\pi^2$ as, $f_{con} = c$, $f_{lin} = a\, m_\pi^2 + b$, $f_{quad} = a\, m_\pi^4 + b\, m_\pi^2 + c$, where $a$, $b$ and $c$ are the fit parameters.

Table 1.1: Extrapolated results of charge radii and magnetic moments.

| | $\langle r^2_{E,\Sigma_c^{++}}\rangle$ | $\langle r^2_{E,\Xi_{cc}^{++}}\rangle$ | $\langle r^2_{E,\Omega_{cc}^{+}}\rangle$ | $\langle r^2_{M,\Sigma_c^{++}}\rangle$ | $\langle r^2_{M,\Sigma_c^{0}}\rangle$ | $\langle r^2_{M,\Omega_c^{0}}\rangle$ | |
|---|---|---|---|---|---|---|---|
| Lin. Fit | 0.192(22) | 0.136(8) | 0.032(6) | 0.410(81) | 0.377(75) | 0.297(33) | |
| Quad. Fit | 0.234(37) | 0.165(12) | 0.043(11) | 0.696(153) | 0.650(126) | 0.354(54) | |
| | $\langle r^2_{M,\Xi_{cc}^{+}}\rangle$ | $\langle r^2_{M,\Omega_{cc}^{+}}\rangle$ | $\mu_{\Sigma_c^{++}}$ | $\mu_{\Sigma_c^{0}}$ | $\mu_{\Omega_c^{0}}$ | $\mu_{\Xi_{cc}^{+}}$ | $\mu_{\Omega_{cc}^{+}}$ |
| Lin. Fit | 0.135(10) | 0.135(11) | 1.569(253) | -0.852(133) | -0.608(45) | 0.411(15) | 0.405(13) |
| Quad. Fit | 0.154(19) | 0.148(21) | 2.220(505) | -1.073(269) | -0.639(88) | 0.425(29) | 0.413(24) |

Our results show that the doubly charged $\Sigma_c^{++}$ has the largest electric charge radius amongst the baryons that we considered. The electric charge radii of $\Omega_{cc}^{+}$ and $\Xi_{cc}^{+}$ [2] are about the same size which suggests that electric charge radius is insensitive to replacing the light $d$-quark by an $s$-quark. We observe that the electric charge radii is much smaller compared to that of the proton (the PDG value is $\langle r^2_{E,p}\rangle$ =0.770 fm$^2$ [13]). The magnetic charge radii of $\Sigma_c^{++}$ and $\Sigma_c^{0}$ are close to that of the proton's, which is $\langle r^2_{M,p}\rangle$ = 0.604 fm$^2$ [13]. The $m_\pi^2$ dependence of the electric and magnetic charge radii's seems to be better modelled by a quadratic fit compared to the other fit models that we considered. A magnetic charge radii extrapolation plot is given in Figure 1.3a. The charge radii of the $\Omega_c$ and $\Omega_{cc}$ baryons, as apparent in Fig. 1.3b for the electric charge radius case, show peculiar fluctuations with respect to the light-quark masses even though they don't contain valance light-quarks. Such behaviour remains as an open question. On the other hand, Fig. 1.3c shows that their magnetic moments are free from such behaviour

and nicely modelled by a linear fit. We refer the reader to Ref. [9] for a more detailed discussion and all the plots.

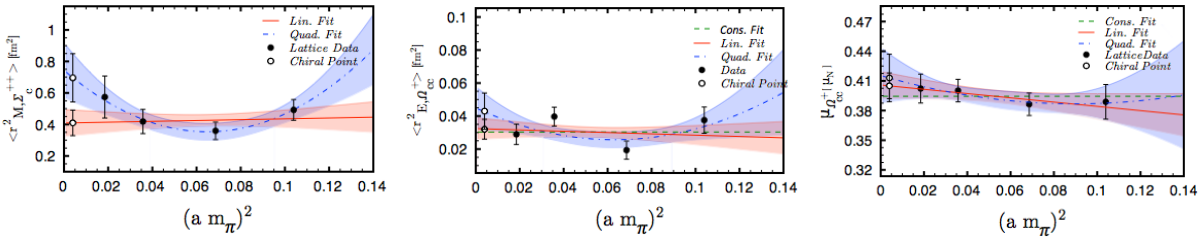


(a) (b) (c)

Figure 1.3: Select chiral extrapolations. a) Magnetic charge radii of $\Sigma_c^{++}$, b) Electric charge radii of $\Omega_{cc}^{+}$, c) magnetic moment of $\Omega_{cc}^{+}$. We show the fits to constant, linear and quadratic forms. The shaded regions are the maximally allowed error regions for the fit forms.

Analysing the individual quark contributions [9] we see that the the charm quark contributions are independent of the quark content of the baryons and the contributions from the $u/d$- and $s$-quark are roughly the same, thus leading $\Sigma_c^{++}$ and $\Xi_{cc}^{++}$, as well as, $\Omega_{cc}^{+}$ and $\Xi_{cc}^{+}$ to have almost the same sizes. The small contribution of $c$ quark suggests that the centre of mass is shifted towards it and this causes the baryon to shrink even though the light quark contributions are systematically larger. The dominant contribution to the magnetic moments come from the doubly represented quarks and the opposite signs of the light and heavy quark contributions suggest that their spins are generally anti-aligned within the baryon. $\Sigma_c^{++}$ has the largest magnetic moment of all and the strange baryons $\Omega_c$ and $\Omega_{cc}$ have somewhat smaller moments. It is interesting to compare these values with the experimental magnetic moment of the proton, which is $\mu_p = 2.793\ \mu_N$ [13]. Comparing our magnetic moment results with several other models we see a quantitative disagreement even though the signs match [9].

## 1.4 Conclusions

We have calculated the electromagnetic form factors of the $\Sigma_c$, $\Omega_c$, $\Xi_{cc}$, $\Omega_{cc}$ baryons and extracted their electric and magnetic charge radii and the magnetic moments from 2+1-flavor simulations of QCD on a $32^3 \times 64$ lattice. Our results imply that the charmed baryons are compact with respect to baryons that are composed of only light quarks, *e.g.*, the proton. The existence of the heavy quark shrinks the baryons and doubly charmed baryons are more compact than the singly charmed baryons of the same charge. The magnetic moments are dominantly determined by the doubly represented quarks. The signs of the magnetic moments are correctly reproduced on the lattice. However, in

general we see an underestimation of the magnetic moments as compared to what has been found with other theoretical methods. A work is underway on nearly physical-point ensembles.

# Chapter 2

# Spin-3/2 Baryons

## 2.1 Introduction

This work extends our previous form factor calculation of spin-1/2 charmed baryons [14] to the spin-3/2 baryons composed of strange and charm quarks. Our aim is to broaden the perspective on heavy baryons by including the elastic electromagnetic form factors of the $J = \frac{3}{2}^+$ strange-charmed baryons and examining the spin-dependence of the quark dynamics. We compute the electromagnetic form factors of the $\Omega$, $\Omega_c^*$, $\Omega_{cc}^*$ and $\Omega_{ccc}$ baryons as well as the $\Omega_c$, $\Omega_{cc}$ baryons with $J = \frac{1}{2}^+$. We extract the electric charge radii and the magnetic moments, and give a thorough comparison of both for the spin-3/2 and spin-1/2 sectors, which helps to improve our understanding of the nonperturbative structure of the strange-charmed baryons.

## 2.2 Theoretical formulation and lattice setup

Electromagnetic form factors of baryons can be calculated through their matrix elements of the electromagnetic vector current $j_\mu = \sum_q e_q \bar{q}(x)\gamma_\mu q(x)$, where $q$ runs over the quark content of the baryon in consideration. We refer the reader to Ref. [14] for the analytical expressions of spin-1/2 baryons. Here we only give the details for spin-3/2 baryons.

The electromagnetic transition matrix element for the spin-3/2 baryons can be written as

$$\langle B_\sigma(p', s')|j_\mu|B_\tau(p, s)\rangle = \sqrt{\frac{M_B^2}{E\,E'}}\bar{u}_\sigma(p', s')\mathcal{O}^{\sigma\mu\tau}u_\tau(p, s), \tag{2.1}$$

where $p(s)$ and $p'(s')$ denote the four momentum (spin) of the initial and final states,

respectively. $M_B$ is the mass of the baryon, $E$ ($E'$) is the energy of the incoming (outgoing) baryon state and $u_\alpha(p,s)$ is the baryon spinor in the Rarita-Schwinger formalism. The tensor in Eq. (2.1) can be written in a Lorentz-covariant form as [15]

$$\mathcal{O}^{\sigma\mu\tau} = -g^{\sigma\tau}\left\{a_1\gamma^\mu + \frac{a_2}{2M_B}P^\mu\right\} - \frac{q^\sigma q^\tau}{(2M_B)^2}\left\{c_1\gamma^\mu + \frac{c_2}{2M_B}P^\mu\right\}, \tag{2.2}$$

where $P = p + p'$ and $q = p' - p$. The multipole form factors we calculate in this work are defined in terms of the covariant vertex functions $a_1$, $a_2$, $c_1$ and $c_2$ as,

$$G_{E0}(q^2) = (1+\frac{2}{3}\tau)\left\{a_1 + (1+\tau)a_2\right\} - \frac{1}{3}\tau(1+\tau)\left\{c_1 + (1+\tau)c_2\right\}, \tag{2.3}$$

$$G_{E2}(q^2) = \left\{a_1 + (1+\tau)a_2\right\} - \frac{1}{2}(1+\tau)\left\{c_1 + (1+\tau)c_2\right\}, \tag{2.4}$$

$$G_{M1}(q^2) = (1+\frac{4}{3}\tau)a_1 - \frac{2}{3}\tau(1+\tau)c_1, \tag{2.5}$$

with $\tau = -q^2/(2M_B)^2$. These multipole form factors are referred to as electric-charge ($E0$), electric-quadrupole ($E2$) and magnetic-dipole ($M1$) multipole form factors.

We calculate the appropriate three-point correlation function on the lattice,

$$\langle G^{Bj^\mu B}_{\sigma\tau}(t_2,t_1;\mathbf{p}',\mathbf{p};\Gamma)\rangle = -i\sum_{\mathbf{x_2},\mathbf{x_1}} e^{-i\mathbf{p}'\cdot\mathbf{x_2}} e^{i\mathbf{q}\cdot\mathbf{x_1}}\Gamma^{\alpha\alpha'}\langle \mathrm{vac}|T[\eta^\alpha_\sigma(x_2)j_\mu(x_1)\bar{\eta}^{\alpha'}_\tau(0)]|\mathrm{vac}\rangle, \tag{2.6}$$

where the $\eta_\mu$ are the baryon interpolating fields chosen similarly to those of $\Delta$ baryon as $\eta_\mu(x) = \frac{1}{\sqrt{3}}\epsilon^{ijk}\{2[q_1^{Ti}(x)C\gamma_\mu q_2^j(x)]q_3^k(x) + [q_1^{Ti}(x)C\gamma_\mu q_3^j(x)]q_2^k(x)\}$. $i$, $j$, $k$ denote the color indices and $C = \gamma_4\gamma_2$. $q_1$, $q_2$, $q_3$ are the quark flavors and taken as $(q_1,q_2,q_3) = \{(s,s,s)$, $(s,s,c)$, $(s,c,c)$, $(c,c,c)\}$ for $\Omega$, $\Omega_c^*$, $\Omega_{cc}^*$ and $\Omega_{ccc}$ baryons, respectively. Spin projections with $\Gamma_4 = \frac{1}{4}(1+\gamma_4)$ and $\Gamma_i = \frac{1}{2}\begin{pmatrix}\sigma_i & 0\\ 0 & 0\end{pmatrix}$ isolate the electric E0, E2 and magnetic M1 multipole form factors. In order to extract the matrix elements, we form a ratio of three-point to two-point functions which, in the large time limit $t_2 - t_1 \gg a$ and $t_1 \gg a$, forms a time-independent ratio free from the unknown overlaps and exponential factors:

$$R_\sigma{}^\mu{}_\tau(t_2,t_1;\mathbf{p}',\mathbf{p};\Gamma) \xrightarrow[t_2-t_1\gg a]{t_1\gg a} \left(\frac{E_p+M_B}{2E_p}\right)^{1/2}\left(\frac{E_{p'}+M_B}{2E_{p'}}\right)^{1/2}\Pi_\sigma{}^\mu{}_\tau(\mathbf{p}',\mathbf{p};\Gamma). \tag{2.7}$$

The multipole form factors can be extracted by using the following combinations of $\Pi_\sigma{}^\mu{}_\tau(\mathbf{p}',\mathbf{p};\Gamma)$ [16]:

$$G_{E0}(q^2) = \frac{1}{3}\left(\Pi_1{}^4{}_1(\mathbf{q}_i,0;\Gamma_4) + \Pi_2{}^4{}_2(\mathbf{q}_i,0;\Gamma_4) + \Pi_3{}^4{}_3(\mathbf{q}_i,0;\Gamma_4)\right), \tag{2.8}$$

$$G_{E2}(q^2) = 2\frac{M(E+M)}{|\mathbf{q}_i|^2}\left(\Pi_1{}^4{}_1(\mathbf{q}_i,0;\Gamma_4) + \Pi_2{}^4{}_2(\mathbf{q}_i,0;\Gamma_4) - 2\Pi_3{}^4{}_3(\mathbf{q}_i,0;\Gamma_4)\right), \tag{2.9}$$

$$G_{M1}(q^2) = -\frac{3}{5}\frac{E+M}{|\mathbf{q}_1|^2}\left(\Pi_1{}^3{}_1(\mathbf{q}_1,0;\Gamma_2) + \Pi_2{}^3{}_2(\mathbf{q}_1,0;\Gamma_2) + \Pi_3{}^3{}_3(\mathbf{q}_1,0;\Gamma_2)\right), \tag{2.10}$$

where $i = 1, 2, 3$ and $\mathbf{q}_i$ are the momentum vectors in three spatial directions.

We run our simulations on $32^3 \times 64$, 2+1-flavor configurations generated by the PACS-CS Collaboration [4] using the Clover fermion action and the Iwasaki gauge action. We use the gauge configurations at $\beta = 1.90$ with the Clover coefficient $c_{SW} = 1.715$, which give a lattice spacing of $a = 0.0907(13)$ fm ($1/a = 2.176(31)$ GeV). The simulations are carried out on almost physical point ensembles with hopping parameter, $\kappa_{u,d}^{sea}$, $\kappa_{u,d}^{val}$=0.13781, which correspond to a pion mass of approximately 156 MeV. The strange quark mass is fixed to $\kappa_{sea}^{s} = 0.13640$. In order to be consistent with the sea quarks we use the clover action for the $s$ valence quark propagators and we take $\kappa_{sea}^{s} = \kappa_{val}^{s}$.

For the charm quarks, we apply the Fermilab method [5] in the form employed by the Fermilab Lattice and MILC Collaborations [6, 7]. In this simplest form of the Fermilab method, the clover coefficients $c_E$ and $c_B$ in the action are set to the tadpole-improved value $1/u_0^3$, where $u_0$ is the average link. Following the approach in Ref. [8], we estimate $u_0$ to be the fourth root of the average plaquette. We tuned the charm-quark hopping parameter to $\kappa_c = 0.1246$ by comparing the experimental spin-averaged static masses of charmonium and heavy-light mesons with our lattice results [14].

We make our simulations with the lowest allowed lattice momentum transfer $q = 2\pi/(N_s a)$, where $N_s$ is the spatial dimension of the lattice and $a$ is the lattice spacing. This corresponds to three-momentum squared value of $\mathbf{q}^2 = 0.183$ GeV$^2$. In order to increase statistics, we insert all possible momentum components, namely $(|q_x|, |q_y|, |q_z|)$ $= (-1,0,0),\ (0,-1,0),\ (0,0,-1),\ (1,0,0),\ (0,1,0),\ (0,0,1)$. We also consider vector-current and spin projections along all spatial directions and take into account all Lorentz components of the Rarita-Schwinger field. By the wall method [1] that we employ, it is possible to extract all the components and simultaneously study all the hadrons we are considering without extra propagator inversions. The source interpolating fields are Gaussian smeared in a gauge-invariant manner and the source-sink separation is chosen to be 12 lattice units in the temporal direction. The smearing parameters for the $s$ quark are chosen so as to give a root-mean-square radius of $\langle r_l \rangle \sim 0.5$ fm. As for the charm quark, we adjust the smearing parameters to obtain $\langle r_c \rangle = \langle r_l \rangle/3$. All statistical errors are estimated by a single-elimination jackknife analysis. We calculate the connected diagrams only and consider the point-split lattice current, $j_\mu = 1/2[\bar{q}(x+\mu)U_\mu^\dagger(1+\gamma_\mu)q(x) - \bar{q}(x)U_\mu(1-\gamma_\mu)q(x+\mu)]$, which is conserved by Wilson fermions.

## 2.3 Results and Discussion

Masses of the $\Omega$, $\Omega_c^{(*)}$, $\Omega_{cc}^{(*)}$ and $\Omega_{ccc}$ baryons are extracted from the shell-source/point-sink lattice two-point function by a simultaneous fit to all spatial Lorentz components. In units of GeV we find, $m_{\Omega_c} = 2.783(13)$, $m_{\Omega_{cc}} = 3.747(10)$ , $m_{\Omega} = 1.790(17)$, $m_{\Omega_c^*} = 2.837(18)$, $m_{\Omega_{cc}^*} = 3.819(10)$ and $m_{\Omega_{ccc}} = 4.769(6)$. For the $\Omega$, $\Omega_c$ and $\Omega_c^*$ baryons there is a discrepancy of around 100 MeV compared to their experimental values, mainly due to the $\kappa_s^{val} = 0.13640$, which we choose same as the $\kappa_s^{sea}$. For instance, $m_\Omega$ is in agreement with the $m_\Omega = 1.772(7)$ GeV reported by the PACS-CS Collaboration [4]. Mass of the $\Omega_{ccc}$ as obtained in our simulations agrees with those from other lattice simulations [17–20] with different actions, which can be taken as a good indicator for the aptness of the charm-quark action we employ.

In our simulations we evaluate each quark sector separately and normalise to unit charge contributions. The baryon properties are then estimated by combining the quark contributions with their weights from respective quark numbers and electric charges as, $\langle\mathcal{O}\rangle = N_s e_s \langle\mathcal{O}_s\rangle + N_c e_c \langle\mathcal{O}_c\rangle$, where $\langle\mathcal{O}\rangle$ is the observable, $N_q$ is the number quarks inside the baryon having flavor $q$ and $e_q$ is the electric charge of the quark. Multipole form factor values are extracted by searching for plateau regions of the ratio given in Eq.(2.7). We refer the reader to Ref. [21] for the illustration of ratios and the fit regions of the $E0$, $M1$ and $E2$ form factors. Here we only quote the charge radii, magnetic moments and quadrupole moments.

Electric charge radii of the baryons are calculated by, $\langle r_E^2\rangle = -6\frac{d}{dQ^2}G_{E0}(Q^2)|_{Q^2=0}$. We assume a dipole form Ansatz for the form factor, $G_{E0}(Q^2) = \frac{G_{E0}(0)}{(1+Q^2/\Lambda^2)^2}$, where $\Lambda$ is the dipole mass. Since we perform our simulations with a single value of the finite momentum transfer, we extract the charge radii using the expression, $\frac{\langle r_E^2\rangle}{G_{E0}(0)} = \frac{12}{Q^2_{min}}\left(\sqrt{\frac{G_{E0}(0)}{G_{E0}(Q^2_{min})}} - 1\right)$. Our numerical values for the electric charge radii are given in Table 2.1. Note that the quark sector contributions are for individual quarks of unit electric charge.

| | $\Omega_c$ | $\Omega_{cc}$ | $\Omega$ | $\Omega_c^*$ | $\Omega_{cc}^*$ | $\Omega_{ccc}$ |
|---|---|---|---|---|---|---|
| $\langle r_E^2\rangle_s$ [fm$^2$] | 0.329(25) | 0.313(16) | 0.326(21) | 0.345(17) | 0.348(16) | — |
| $\langle r_E^2\rangle_c$ [fm$^2$] | 0.064(11) | 0.073(4) | — | 0.062(5) | 0.078(3) | 0.084(3) |
| $\langle r_E^2\rangle$ [fm$^2$] | -0.177(18) | 0.026(4) | -0.326(21) | -0.189(12) | -0.012(6) | 0.168(5) |

Table 2.1: Electric charge radii of the $\Omega$, $\Omega_c^*$, $\Omega_{cc}^*$ and $\Omega_{ccc}$. Results are given in fm$^2$. Quark sector contributions are for single quark and normalised to unit charge. Total electric charge radius of the spin-1/2 $\Omega_c$ is estimated by combining quark sectors since its electric form factor vanishes due to its zero electric charge.

We observe that the $s$-quark contribution to the electric charge radii is almost independent of the quark-flavor composition of the baryon. The charge radii of both spin-1/2 and spin-3/2 baryons agree within one standard deviation, which can be seen more clearly in Fig. 2.1. In the case of $c$-quark contributions, the charge radii of all baryons are similar. The ratios of individual quark-flavor contributions in the spin-1/2 to that in the spin-3/2 sector are also shown in Fig. 2.1. We observe that for the singly-charmed $\Omega_c$ baryon, $s$- and $c$-quark charge distributions are insensitive to the spin-flip of the $c$-quark whereas in the case of the doubly-charmed $\Omega_{cc}$ baryon the contributions of $s$- and $c$-quark to the charge radii increase. We find the electric charge radius of the $\Omega$ baryon to be $\langle r_E^2 \rangle_{\Omega^-} = -0.326(21)$ fm$^2$ in quite good agreement with the previous lattice determinations [11, 16]. A comparison of baryon charge radii is made in Fig. 2.1. In magnitude, $\Omega$ ($\Omega_c^*$) baryon has the largest electric charge radius among all (spin-3/2) baryons we study. Spin-1/2 (spin-3/2) $\Omega_c$ ($\Omega_c^*$) and $\Omega_{ccc}$ seem to have similar charge radii while the $\Omega_{cc}$ ($\Omega_{cc}^*$) baryon has almost a vanishing charge radius.

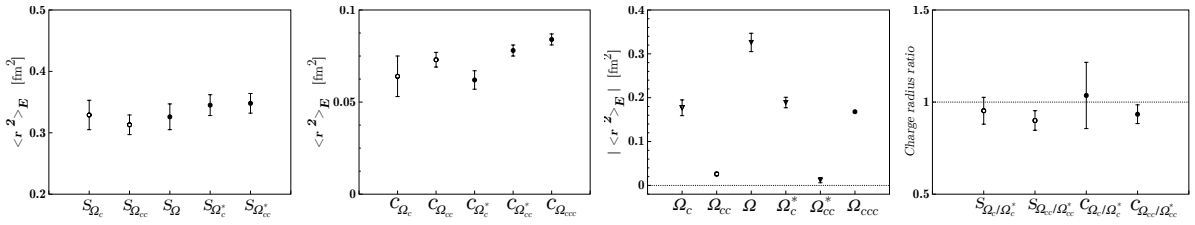


Figure 2.1: *First three are:* $s-$ and $c-$quark contributions to the electric charge radii and the total electric charge radii of the denoted baryons respectively. *Last one is:* the ratio of the quark contribution to the electric charge radii of the spin-1/2 $\Omega_c$, $\Omega_{cc}$ to spin-3/2 $\Omega$, $\Omega_c^*$ baryons. Absolute values are shown for a better comparison. Data points denoted by a triangle indicates a negative value. Empty symbols indicate the spin-1/2 sector.

We evaluate the magnetic dipole moment in units of nuclear magnetons as, $\mu_B = G_{M1}(0)\frac{e}{2m_B} = G_{M1}(0)\frac{m_N}{m_B}\mu_N$, where $m_N$ is the physical nucleon mass and $m_B$ is the baryon mass as obtained on the lattice. As in Ref. [22], we assume that the momentum-transfer dependence of the magnetic dipole form factor is same as the momentum dependence of the respective baryon's charge form factor. For instance, the scaling of $G_{M1}$ is given by, $G_{M1}^{s,c}(0) = G_{M1}^{s,c}(q^2)\frac{G_E^{s,c}(0)}{G_E^{s,c}(q^2)}$, where we consider the scaling of $s$ and $c$ quark sectors separately since each sector has a different scaling property. Quark sectors are then combined to construct $G_{M1}(0)$.

Our numerical values for the magnetic moments are listed in Table 2.2, which are also illustrated in Fig. 2.2. We find for spin-1/2 baryons that the contribution of a single quark to the magnetic moment significantly increases when it is doubly represented. The effect of the spin flip is seen as a sign change in case of the $\Omega_c$ and $\Omega_{cc}$ baryons. We illustrate the ratios of the quark-sector contributions to spin-1/2 and spin-3/2 baryons in

| | $\Omega_c$ | $\Omega_{cc}$ | $\Omega$ | $\Omega_c^*$ | $\Omega_{cc}^*$ | $\Omega_{ccc}$ |
|---|---|---|---|---|---|---|
| $\mu_s$ $[\mu_N]$ | 0.979(47) | -0.402(17) | 1.533(55) | 1.453(36) | 1.408(29) | — |
| $\mu_c$ $[\mu_N]$ | -0.092(6) | 0.216(3) | — | 0.358(8) | 0.352(4) | 0.338(2) |
| $\mu$ $[\mu_N]$ | -0.688(31) | 0.403(7) | -1.533(55) | -0.730(23) | 0.000(10) | 0.676(5) |

Table 2.2: Magnetic moments of the $\Omega$, $\Omega_c^{(*)}$, $\Omega_{cc}^{(*)}$ and $\Omega_{ccc}$. Results are given in units of nuclear magnetons, $\mu_N$. Quark sector contributions are for single quark and normalised to unit charge.

Fig. 2.2 to understand the effect of the quark spin configurations on the quark magnetic moments better. In the case of spin-3/2 baryons, both the individual $s$-quark and $c$-quark contributions are enhanced. Ratios, $S_{\Omega_c'\Omega_c^*}$, and $C_{\Omega_{cc}'\Omega_{cc}^*}$, are consistent with each other like the singly strange and the singly charmed baryon ratios, suggesting that the difference between the spin-1/2 and the spin-3/2 baryons is almost independent of the quark flavour. We find the magnetic moment of the $\Omega^-$ baryon to be $\mu_{\Omega^-} = -1.533 \pm 0.055\ \mu_N$, which is smaller in magnitude than the experimental value, $\mu_{\Omega^-}^{exp} = -2.02 \pm 0.05\ \mu_N$ [23]. One of the reasons for this discrepancy can arise from the difference between our $m_\Omega = 1.790(17)$ and the experimental value, $m_\Omega = 1.673(29)$, which is around 7%. Compared to the other lattice determinations that use the three-point function method, our value is slightly smaller (in magnitude) than the quenched result, $\mu_{\Omega^-} = -1.697 \pm 0.065\ \mu_N$, of Boinepalli et.al [16] and agrees with the Alexandrou et.al's extrapolated value, $\mu_{\Omega^-} = -1.875 \pm 0.399$ $\mu_N$ [11] within one sigma error. In Ref.[24] magnetic moment of $\Omega$ has determined to be $\mu_{\Omega^-} = -1.93 \pm 0.08$, by a background field method on $m_\pi = 366$ MeV lattices. Magnetic moments of $\Omega_c$ and $\Omega_c^*$ being similar to each other suggests that the spin flip of the charm quark has a small effect, in accord with heavy-quark spin symmetry expectations. From a quark-model approach one would expect the magnetic moment of $\Omega_c$ ($\Omega_{cc}$) to be similar in magnitude to that of $\Omega_c^*$ ($\Omega_{cc}^*$)'s. Such an expectation is consistent with our $\Omega_c$ findings, however, the magnetic moments of $\Omega_{cc}$ and $\Omega_{cc}^*$ differ drastically, the latter having a completely vanishing magnetic moment. The difference between the $\Omega_c$ and $\Omega_c^*$ is that the $c$-quark is anti-aligned with the $ss$ component in $\Omega_c$ whereas it is aligned in $\Omega_c^*$. Combined with their electric charges, quark sectors add constructively for $\Omega_c$ and destructively for $\Omega_c^*$. These two different behaviours occur in such a balanced way that the magnetic moments of the $\Omega_c$ and $\Omega_c^*$ end up to be similar. In case of the doubly-charmed $\Omega_{cc}$ and $\Omega_{cc}^*$ however, the interplay between the electric charges and the number of quarks breaks the balance and lead to magnetic moments for $\Omega_{cc}$ and $\Omega_{cc}^*$ that differ significantly.

The electric-quadrupole form factors of spin-3/2 baryons provide information about the deviation of the baryon shape from spherical symmetry. In the Breit frame, the quadrupole form factor and the electric charge distribution are related as [25], $G_{E2}(0) =$

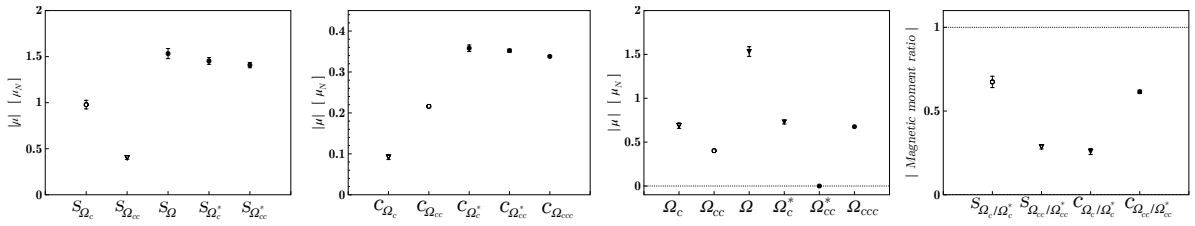

Figure 2.2: Same as Fig.1 but for magnetic moments.

$M_B^2 \int d^3r\bar{\psi}(r)(3z^2 - r^2)\psi(r)$, where $3z^2 - r$ is the standard operator used for quadrupole moments. A positively charged baryon has a prolate (oblate) charge distribution when quadrupole form factor is positive (negative). As in the case of the $E0$ and $M1$ form factors, we estimate the $E2$ form factor by the plateau approach. We compute and extract the $s$- and $c$-quark sector contributions individually. Unfortunately, low signal/noise ratio does not allow us to conclude about $\Omega$ and $\Omega_c^*$ baryons. In the case of the heavier $\Omega_{cc}^*$ and $\Omega_{ccc}$ baryons, however, we find $E_2(Q^2)^{\Omega_{cc}^*} = -0.310(128)$ and $E_2(Q^2)^{\Omega_{ccc}} = -0.273(76)$ indicating that their charge distributions deform to an *oblate* shape.

## 2.4 Summary

We have calculated the electromagnetic form factors of the $\Omega$, $\Omega_c^*$, $\Omega_{cc}^*$ and $\Omega_{ccc}$ baryons at the lowest allowed three-momentum value ($\mathbf{q}^2 = 0.183$ GeV$^2$) and extracted their electric charge radii, magnetic moments and quadrupole moments on almost physical point gauge configurations. Same quantities for the $\Omega_c$ and $\Omega_{cc}$ baryons are also computed. For each observable we have identified the quark sector contributions and gave a comparison between the quark sectors and spin-1/2 and spin-3/2 sectors. In addition, baryon properties are constructed from the individual quark sectors contributions.

# Bibliography


[1] K.U. Can, G. Erkol, M. Oka, A. Ozpineci, and T.T. Takahashi. Vector and axial-vector couplings of D and D* mesons in 2+1 flavor Lattice QCD. *Phys.Lett.*, B719:103–109, 2013. doi:10.1016/j.physletb.2012.12.050.

[2] K.U. Can, G. Erkol, B. Isildak, M. Oka, and T.T. Takahashi. Electromagnetic properties of doubly charmed baryons in Lattice QCD. *Phys.Lett.*, B726:703–709, 2013. doi:10.1016/j.physletb.2013.09.024.

[3] C. Alexandrou, M. Brinet, J. Carbonell, M. Constantinou, P.A. Harraud, et al. Nucleon electromagnetic form factors in twisted mass lattice QCD. *Phys.Rev.*, D83:094502, 2011. doi:10.1103/PhysRevD.83.094502.

[4] S. Aoki et al. 2+1 Flavor Lattice QCD toward the Physical Point. *Phys. Rev.*, D79:034503, 2009. doi:10.1103/PhysRevD.79.034503.

[5] Aida X. El-Khadra, Andreas S. Kronfeld, and Paul B. Mackenzie. Massive Fermions in Lattice Gauge Theory. *Phys. Rev.*, D55:3933–3957, 1997. doi:10.1103/PhysRevD.55.3933.

[6] T. Burch, C. DeTar, M. Di Pierro, A.X. El-Khadra, E.D. Freeland, et al. Quarkonium mass splittings in three-flavor lattice QCD. *Phys.Rev.*, D81:034508, 2010. doi:10.1103/PhysRevD.81.034508.

[7] C. Bernard et al. Tuning Fermilab Heavy Quarks in 2+1 Flavor Lattice QCD with Application to Hyperfine Splittings. *Phys.Rev.*, D83:034503, 2011. doi:10.1103/PhysRevD.83.034503.

[8] Daniel Mohler and R.M. Woloshyn. $D$ and $D_s$ meson spectroscopy. *Phys.Rev.*, D84:054505, 2011. doi:10.1103/PhysRevD.84.054505.

[9] K.U. Can, G. Erkol, B. Isildak, M. Oka, and T.T. Takahashi. Electromagnetic structure of charmed baryons in Lattice QCD. 2013.

[10] C. Alexandrou et al. Axial Nucleon form factors from lattice QCD. *Phys.Rev.*, D83:045010, 2011. doi:10.1103/PhysRevD.83.045010.

[11] C. Alexandrou, T. Korzec, G. Koutsou, J.W. Negele, and Y. Proestos. The Electromagnetic form factors of the $\Omega^-$ in lattice QCD. *Phys.Rev.*, D82:034504, 2010. doi:10.1103/PhysRevD.82.034504.

[12] L. Maiani, G. Martinelli, M. L. Paciello, and B. Taglienti. SCALAR DENSITIES AND BARYON MASS DIFFERENCES IN LATTICE QCD WITH WILSON FERMIONS. *Nucl. Phys.*, B293:420, 1987.

[13] J. Beringer and Particle Data Group. Review of particle physics. *Phys. Rev. D*, 86:010001, Jul 2012. doi:10.1103/PhysRevD.86.010001.

[14] K.U. Can, G. Erkol, B. Isildak, M. Oka, and T.T. Takahashi. Electromagnetic structure of charmed baryons in Lattice QCD. *JHEP*, 1405:125, 2014. doi:10.1007/JHEP05(2014)125.

[15] S. Nozawa and D.B. Leinweber. Electromagnetic form-factors of spin 3/2 baryons. *Phys.Rev.*, D42:3567–3571, 1990. doi:10.1103/PhysRevD.42.3567.

[16] S. Boinepalli, D. B. Leinweber, P. J. Moran, A. G. Williams, J. M. Zanotti, and J. B. Zhang. Electromagnetic structure of decuplet baryons towards the chiral regime. *Phys. Rev. D*, 80:054505, Sep 2009. doi:10.1103/PhysRevD.80.054505. URL `http://link.aps.org/doi/10.1103/PhysRevD.80.054505`.

[17] Y. Namekawa et al. Charmed baryons at the physical point in 2+1 flavor lattice QCD. *Phys.Rev.*, D87:094512, 2013. doi:10.1103/PhysRevD.87.094512.

[18] C. Alexandrou, V. Drach, K. Jansen, C. Kallidonis, and G. Koutsou. Baryon spectrum with $N_f = 2 + 1 + 1$ twisted mass fermions. *Phys.Rev.*, D90(7):074501, 2014. doi:10.1103/PhysRevD.90.074501.

[19] Raul A. Briceno, Huey-Wen Lin, and Daniel R. Bolton. Charmed-Baryon Spectroscopy from Lattice QCD with $N_f = 2 + 1 + 1$ Flavors. *Phys.Rev.*, D86:094504, 2012. doi:10.1103/PhysRevD.86.094504.

[20] Zachary S. Brown, William Detmold, Stefan Meinel, and Kostas Orginos. Charmed bottom baryon spectroscopy from lattice QCD. *Phys. Rev.*, D90(9):094507, 2014. doi:10.1103/PhysRevD.90.094507.

[21] K. U. Can, G. Erkol, M. Oka, and T. T. Takahashi. Look inside charmed-strange baryons from lattice QCD. *Phys. Rev.*, D92(11):114515, 2015. doi:10.1103/PhysRevD.92.114515.

[22] Derek B. Leinweber, Terrence Draper, and R.M. Woloshyn. Baryon octet to decuplet electromagnetic transitions. *Phys.Rev.*, D48:2230–2249, 1993. doi:10.1103/PhysRevD.48.2230.

[23] K.A. Olive and Particle Data Group. Review of particle physics. *Chinese Physics C*, 38 (9):090001, 2014. URL `http://stacks.iop.org/1674-1137/38/i=9/a=090001`.

[24] C. Aubin, K. Orginos, V. Pascalutsa, and M. Vanderhaeghen. Lattice calculation of the magnetic moments of $\Delta$ and $\Omega^-$ baryons with dynamical clover fermions. *Phys. Rev. D*, 79: 051502, Mar 2009. doi:10.1103/PhysRevD.79.051502. URL `http://link.aps.org/doi/10.1103/PhysRevD.79.051502`.

[25] Derek Leinweber, Terrence Draper, and R. Woloshyn. Decuplet baryon structure from lattice qcd. *Phys. Rev. D*, 46:3067–3085, Oct 1992. doi:10.1103/PhysRevD.46.3067. URL `http://link.aps.org/doi/10.1103/PhysRevD.46.3067`.